Design method of water jet pump towards high cavitation performances

L L Cao[1], B X Che, L J Hu, D Z Wu

Institute of Process Equipment, College of Chemical and Biological Engineering, Zhejiang University
Zheda Road 38 #, 310027 Hangzhou, Zhejiang, China

E-mail: caolinlin@zju.edu.cn

Abstract. As one of the crucial components for power supply, the propulsion system is of great significance to the advance speed, noise performances, stabilities and other associated critical performances of underwater vehicles. Developing towards much higher advance speed, the underwater vehicles make more critical demands on the performances of the propulsion system. Basically, the increased advance speed requires the significantly raised rotation speed of the propulsion system, which would result in the deteriorated cavitation performances and consequently limit the thrust and efficiency of the whole system. Compared with the traditional propeller, the water jet pump offers more favourite cavitation, propulsion efficiency and other associated performances. The present research focuses on the cavitation performances of the waterjet pump blade profile in expectation of enlarging its advantages in high-speed vehicle propulsion. Based on the specifications of a certain underwater vehicle, the design method of the waterjet blade with high cavitation performances was investigated in terms of numerical simulation.

Introduction

Developing towards much higher advance speed, the underwater vehicles make more critical demands on the performances of the propulsion system. Basically for the traditional propeller system, the increased advance speed requires the significantly raised rotation speed, which would result in the deteriorated cavitation performances and consequently limit the thrust as well as the efficiency of whole system. Instead of directly increasing the rotation speed, the alternative structures of the propulsion system give more beneficial choices. Distinguished from the traditional propellers which make use of the blade lift to drive, the waterjet pump takes advantages of the momentum difference between the inflow and outflow of the pump to thrust vehicles forward. Hence, under the same design specifications, the water jet pump appears with obviously reduced rotation speed as well as more favourite cavitation and vibration performances.

While further increase the vehicle advance speed, the inherent superiorities in cavitation performances of waterjet pump are also insufficient. Commonly, to relieve the cavitation problem, the underwater vehicles would try to increase their diving depth as well as the substantial pressure during high speed advancing. Plenty of researches have been done to improve the inherent cavitation performances of the waterjet pump. Since the cavitation performances of rotor blade are highly

[1] The correspondence author: Cao Linlin

associated with its pressure distribution, it is essential to make the pressure field optimized but with the blade loading unchanged. The optimization of the inlet condition to raise the inflow static pressure by adjusting the geometries of pump is also effective to avoid or delay the cavitation inception. Thurston and Amsler [4] proposed that it is quite beneficial to narrow the scope between the subcavitating and supercavitating status due to the high instabilities here, and they have made a detailed presentation about the cavitation control methods by adjusting the duct geometries as well as optimizing the inflow static pressure in the waterjet pump. Additionally, the local vortices, the abrupt flow acceleration and other types of flow structures which result in sharp static pressure drop and associated losses also contribute to the cavitation problem significantly. The axial and mixed flow pumps are usually characterized by the tip leakage flows, which are always accompanied with sharp pressure drop as well as cavitation inception inside the vortex cores. Wu et al. [5] simulated the flow vortices structure in the waterjet pump, and carried out the researches on the mechanism and the cavitation inception in the tip leakage vortex. Generally, the loading situation along the span and at the blade tip region must be carefully considered to improve the pump cavitation performances while keeping the work capacities there.

In the present paper, the cavitation performances of the waterjet pump blade profile in high-speed vehicle propulsion are concentrated. Refer to the pump performances under high-speed advance, the blade geometries and associated loading situations were studied to improve the pressure distributions as well as the cavitation performances. Based on the specifications of a certain underwater vehicle, the waterjet blade design method with the consideration of cavitation performances was investigated in terms of numerical simulation.

Key Parameters and Performance Simulation Method of the Waterjet pump

In the present paper, all of the model waterjet pumps were designed and studied based on a certain underwater vehicle with the specifications described in table 1, which could be simplified as an axisymmetric cylindrical body.

Table 1. Major performances specifications of the underwater vehicle

Advance speed [Kn]	Diameter [m]	Length [m]	Thrust [KN]
50	0.324	6	5

Refers to the distribution properties of the wake flow at the vehicle trail [6,7], the inflow profile of the waterjet pump described as equation (1) was specified to simulate the inlet velocity. Herein the axial velocity at the pump inlet V_m [m/s] was assumed to vary linearly against the pump inlet radius D, and the circumferential and radial components are assumed to be negligible.

$$V_m = 73.4D + 7 \quad (1)$$

To offer sufficient power supply to the vehicle while keep the effect to its hydrodynamics properties minimized, the dimension and mechanical structure of propeller must be carefully determined [6]. Since the present paper concentrate on the internal performances of waterjet as the propulsion device, the specifications of the waterjet pump were majorly decided based on the vehicle required thrust and the pump models in other related researches [5,7]. As listed in Table 2, the rotor outer diameter was specified as 67% of that of vehicle, which was supposed to keep the hydrodynamic influence on a relatively low level.

Table 2. Major specifications of the model waterjet pumps

Head rise [m]	20	Blade tip clearance [mm]	0.5

Rotation speed [min^{-1}]	3000	Inlet area [m^2]	0.0278
Flow rate [m^3/s]	0.5477	Outlet area [m^2]	0.0196
Thrust [KN]	5	Rotor hub diameter [m]	0.22
Power [KW]	138	Rotor tip diameter [m]	0.116
Rotor blade number	7	Inflow axial velocity [m/s]	19.70
Stator blade number	11	Outflow axial velocity [m/s]	27.94

In the present study, all of the simulation works were conducted with the commercial Computational Fluid Dynamics (CFD) code ANSYS CFX, and the modelling and computational grid generations were done by ANSYS Turbogrid. The entire annuluses model is illustrated in figure 1 to better visualize the waterjet pump concept. For the preliminary evaluation of the waterjet pump internal and external performances, only the steady-state computations with one rotor-stator passage were carried out. As the most prominent two-equation models proficient in the flow separation predictions, the *k-ω* based SST (Shear Stress Transfer) Model was employed in all of our simulation works.

(a) Entire annuluses model with pump casing

(b) Entire annuluses model without pump casing

Figure 1. Computational model of waterjet pump

Blade Loading Distribution Design Method Based on Cavitation Performances

To evaluate the cavitation performances quantitatively, the definition of Required Net Positive Suction Head (NPSHr) is given in equation (1), in which V_L and W_L are specified as the absolute and the relative velocities at the blade leading edge point 'L', and λ_1 and λ_2 as the loss coefficients decided by the inlet condition and the blade profile respectively.

$$\mathrm{NPSH}_r = \lambda_1 \frac{{C_L}^2}{2g} + \lambda_2 \frac{{W_L}^2}{2g} \tag{2}$$

In the traditional axial flow pump designed with the loading profile of 'free vortex', the cavitation inception is ordinarily found at the leading edge around the tip profile due to the low static pressure as well as the rather high peripheral speed and relative velocity there.

Regardless of the inlet condition, the cavitation performances of rotor blade are highly associated with its pressure distribution, it is essential to make the pressure field optimized but with the blade loading unchanged. Generally, the aerofoil with heavy loading is usually fore-loaded with lowest pressure point and sharp pressure gradient at the Leading Edge (LE) on the Suction Surface (SS), which could offer high work capacity but quite unfavourable to the cavitation performances. In the

present paper, the blade loading situation with the compromise between hydraulic and cavitation performances was studied. Based on the related research results [8-10], the most decisive parameters for the blade loading situation could be concluded as: 1) camber line function, 2) max camber height location x_f/l, 3) incidence angle i.

1.1. Camber line function

In the present study, the quadratic parabola equation (2) was applied to specify the camber geometry, in which a, b, and c respectively denote any arbitrary constants, the chord ratio x ranges from 0 to 1, and θ represents the local gradient angle of the camber curve (as shown in figure 2) with the condition of $tan\,\theta = dy/dx$.

$$\theta(x)=ax^2 + bx + c \tag{3}$$

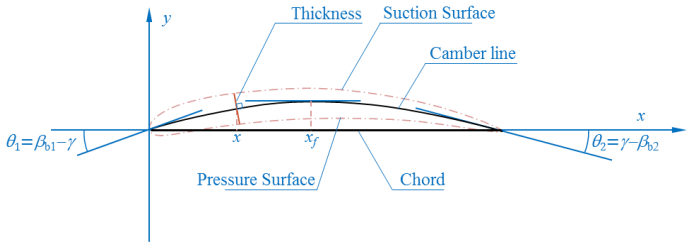

Figure 2. Schematic camber line geometry

1.2. Other factors related to camber geometry

Moreover, the max camber height location x_f/l and the incidence angle i are among the important decisive factors to the blade loading and pressure distribution along the PS and SS, consequently influential to the cavitation performances. The large work capacity is usually accompanied with large attack α and incidence angle i, and the location of x_f/l close to the LE, which ordinarily results in the fore-loading situation. In that case, the SS is characterized by a region with rather low pressure to offer considerable pressure difference as well as large lift force, in which the cavitation inception usually occurs. In the related researches [8, 9], Zangeneh, M. et al. proposed the optimum pressure distribution model for the impellers in terms of secondary flow suppression, and indicated that it is beneficial to respectively increase the blade aft part loading at the hub section and decrease that at the tip area.

Generally, the blade pressure distribution should be optimized with the min pressure raised for the cavitation consideration but the blade loading maintained for the hydraulic performance consideration. The combination of x_f/l, i and other parameters should be carefully specified to get more flat blade loading curve at the SS. In the present research, the several combinations were evaluated for the blade loading situation, hydraulic performances and cavitation performances.

$$\delta = m_c(\beta_{b1} - \beta_{b2})\sigma^{-n_c} \tag{4}$$

$$\delta = \Delta\beta + 13.05\left(\frac{x_f}{l} - 0.4\right) \tag{5}$$

The design specifications of three of these models are given in table 3. For the first two models G1, the classic deviation angle model of equation (4) was adopted, where m_c=0.26, n_c=0.5 as in the axial flow compressors and σ represents the cascade solidity; while for the G2 and G3, to improve the work

capacity as well as the flow turning under the aft-loading situation, an alternative empirical formula equation (5) was applied, which has been validated in the previous researches [11].

Table 3. Design specifications of three of rotor models

Section		1(Hub)	2	3	4	5(Tip)
G1	Incidence [°]	2.00	1.00	1.00	1.00	0.00
	x_f/l	0.40	0.40	0.40	0.40	0.40
	Deviation angle [°]	3.60	3.71	2.54	2.10	1.96
	Attack angle [°]	10.824	7.996	5.368	3.804	2.856
G2	Incidence [°]	2.00	1.00	1.00	1.00	0.00
	x_f/l	0.40	0.45	0.50	0.55	0.60
	Deviation angle [°]	5.00	5.15	4.91	4.95	6.03
	Attack angle [°]	11.898	6.424	3.622	2.079	0.429
G3	Loading coefficient L_c	0.915	1.007	1.060	1.115	1.129
	Incidence [°]	2.00	1.00	1.00	1.00	0.00
	x_f/l	0.500	0.525	0.550	0.575	0.600
	Deviation angle [°]	10	7.10	6.09	5.54	6.03
	Attack angle [°]	7.158	4.114	2.502	1.559	0.429

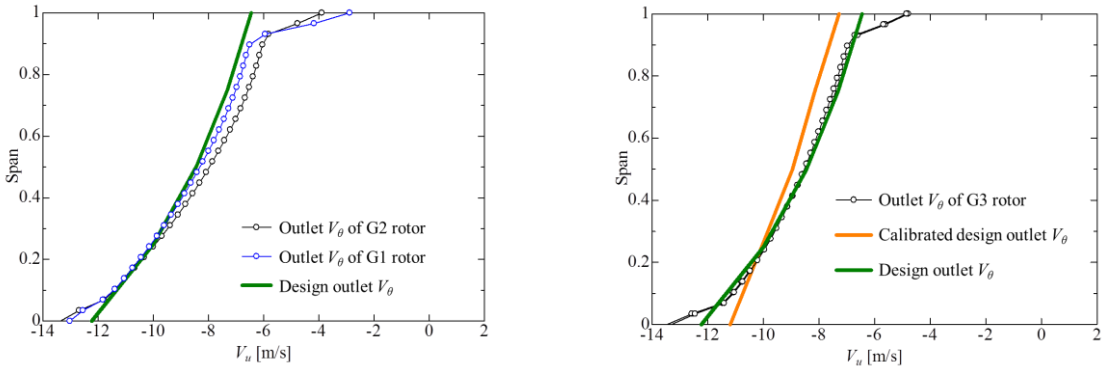

(a) Outlet flow swirl V_θ of G1 and G2 rotors (b) Outlet flow swirl V_θ of G3

Figure 3. Schematic camber line geometry

The third model type G3 was designed based on the simulation results of the first two models. From figure 3(a), it can be seen that expect for the defect due to the tip leakage flow, the distributions of outflow swirl V_θ of G1 and G2 rotors are deviated from the design expectation denoted in green. Compared to the G1 blade designed with x_f/l close to LE (40% of chord length) along the whole span, the G2 rotor shows the more pronounced defect of V_θ with x_f/l moving backward (from 40% at hub to 60% at tip), which indicates the insufficient work capacity of the G2 profile section under the aft-

loading situation. To obtain the flow turning as well as the hydraulic head satisfying the design specification, the loading coefficient L_c was introduced to calibrate the distribution of design head along the blade span. In equation (6), subscript d denotes under design condition, and G2 denotes the simulation results of G2 rotor.

$$L_c = V_{\theta,\mathrm{d}}/V_{\theta,\mathrm{G2}} \tag{6}$$

Combining the calibration methods above, the G3 rotor was obtained as described in table 3. It is clear that compared with those profiles designed with equal x_f/l, G3 showed obviously increased attack angles as well as improved work capacity. In this case, the G3 blade profile was supposed to reach a compromise between the cavitation performances and hydraulic performances.
The thickness evolution law of NACA 4* series [12] as expressed by Eq. (3-16) was adopted,

$$\frac{y_t(x)}{l} = 5\frac{t}{l}\left\{a_0\sqrt{\frac{x}{l}} + a_1\frac{x}{l} + a_2\left(\frac{x}{l}\right)^2 + a_3\left(\frac{x}{l}\right)^3 + a_4\left(\frac{x}{l}\right)^4\right\} \tag{7}$$

where $y_t(x)/l$ represents the relative thickness at any arbitrary position of x/l, and $a_0 \sim a_4$ are given by the NACA4* profile data. With the calculated thickness perpendicularly growing to both sides at the corresponding camber point, the outlines of the pressure and suction surfaces are generated as shown in figure 2.

Hydraulic and Cavitation Performances of Rotor Models
With the steady CFD simulation methods mentioned in Section 2, the preliminary performances of three types of rotors at the design flow rate Q = 0.5477 [m^3/s] as presented in table 4. The properties of cavitation inception of these rotors were studied with the parameter of NPSH$_r$ (Required Net Positive Suction Head), which was calculated under their respective design conditions by the following equation (8),

$$\mathrm{NPSH}_r = \frac{P_{t,1} - P_{min}}{\rho g} \tag{8}$$

where $P_{t,1}$ represents the total pressure at the rotor inlet, and P_{min} the minimum pressure obtained around the blades of each rotor. And the positions with rather low pressure caused by the local vortices and losses were ignored in the evaluation of NPSH$_r$, such as the PS-tip corner where the great pressure drop is induced by the tip leakage flow.

Table 4. External Performances of Three Types of Rotors

	H [m]	η	T [KN]	NPSHr [m]
G1	18.714	90.43%	4.05	37.88
G2	20.080	92.54%	4.27	37.89
G3	20.304	91.70%	4.5	20.74

From the simulation results represented in table 4, it can be seen that even the profile of G1 rotor was designed as fore-loaded, it can hardly meet the design specification due to the insufficient deviation angles at the blade trail. With the deviation angles renewed, the latter two rotors G2 and G3 show well improved head rises, which are highly close to the design specifications H = 20 [m]. Compared with the G2 rotor, the G3 rotor with max camber height location moved backward

represents the well increased P_{min} but can still offer comparable work capacity, which indicates that the G3 blade has the more flat loading curve and do work on the fluid more evenly from LE to TE.

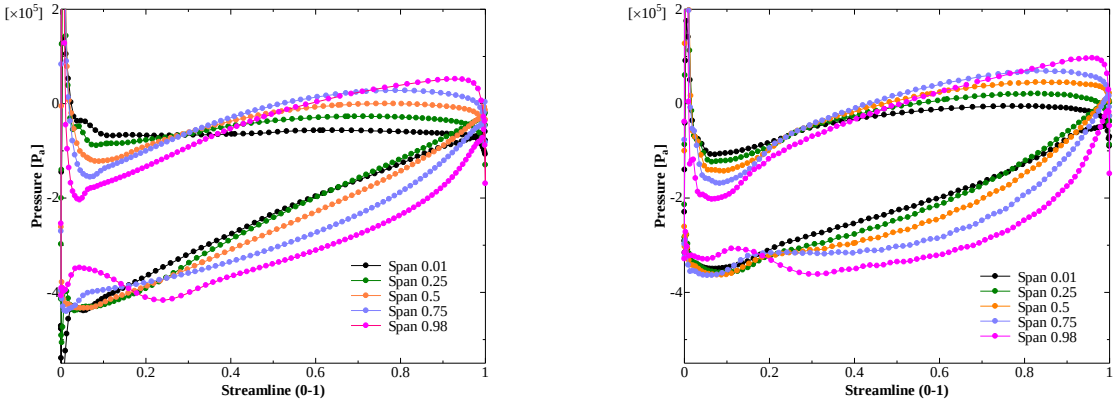

(a) Loading curves of G2 rotor blade (b) Loading curves of G3 rotor blade

Figure 4. Loading curves of G2 and G3 rotor blades

The loading curves of the G2 and G3 rotor blades at various span locations are given in figure 4, from which the above assumption could be validated. In the area near to hub, the G2 blade shows rather steep pressure growing gradient on SS with a region of lowest pressure at LE as shown in figure 4 (a), which implies that the loading of these sections is concentrated at LE. This region usually corresponds to the location where cavitation inception occurs. With the max camber height location moving backward and the calibration of the head distribution in spanwise, the G3 blade shows the aft-loading situation and relatively flat pressure growing curves on SS through the whole span. Hence, the G3 rotor was believed to have well delayed cavitation inception compared with the G2 rotor under the equal ambient pressure.

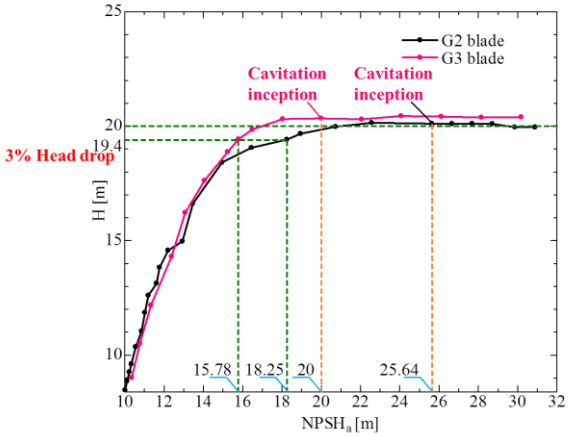

Figure 5. Drop curves of G2 and G3 rotor blades

The drop curves of two rotors are presented in figure 5, which were calculated in steady simulations with cavitation model of Rayleigh Plesset. It can be seen that the G3 rotor blade appears with superior cavitation performances compared to the G2 rotor blade.

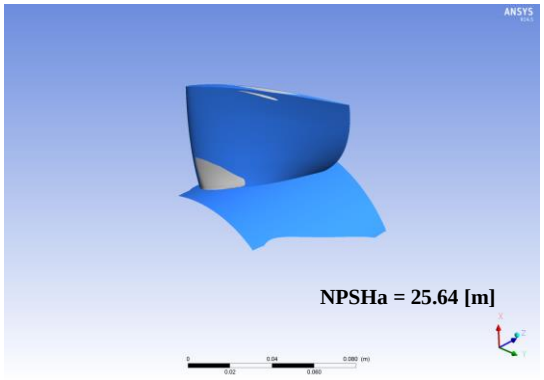

(a) Cavitation inception of G2 rotor blade

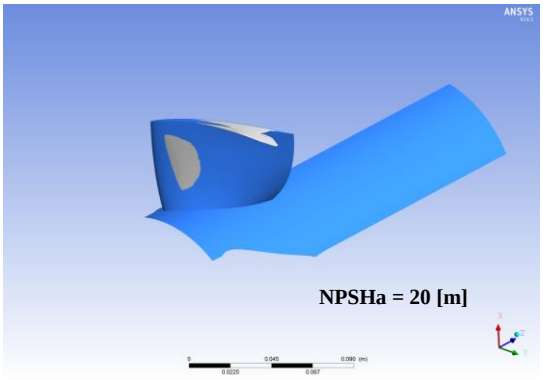

(b) Cavitation inception of G3 rotor blade

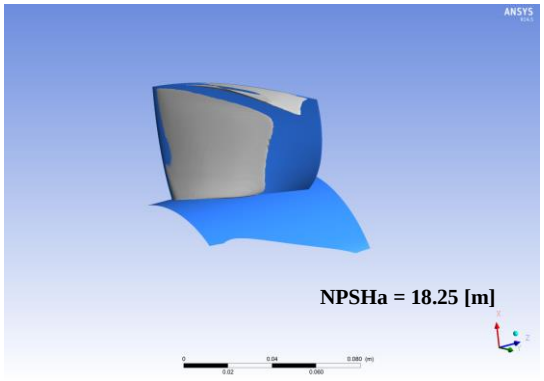

(c) 3% head drop situation of G2 rotor blade

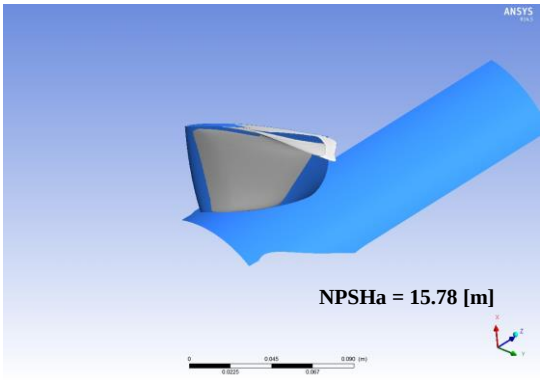

(d) 3% head drop situation of G3 rotor blade

Figure 6. Cavitation visualization of G2 and G3 rotor blades with vapour volume fraction as 10%

In figure 6, the cavitation range under various ambient pressure is presented with the vapour volume fraction of 10% as shown in grey. Regardless of the cavitation occurred in tip leakage flow, due to the different consideration in the design of blade loading, the two rotors differ from each other obviously in the locations of cavitation inception. As shown in figure 5, the G2 rotor was found to have cavitation at LE of the hub section, where the blade loading was designed to be rather large. The G3 rotor with the relatively flat pressure distribution curve at SS shows cavitation inception in the mid part of blade, and with the blade loading distribution optimized the NPSHa at the cavitation inception moment ($NPSH_{a,G3}$ = 20 [m]) is found to be well reduced from that in G2 rotor ($NPSH_{a,G2}$ = 25.64 [m]), indicating the much lower possibility of cavitation under same working condition.

With the ambient pressure further reduced, both two rotors suffer from the hydraulic deterioration as the steep drop of head rise and efficiency. In this paper, the 3% head drop point was determined as the critical cavitation point. As shown in figure 6 (c) and (d), the suction surfaces of both rotor blades are covered with a massive of vapour cloud, and the blade loading is significantly decreased. Even in this case, the G3 rotor blade still shows relatively superior ability to maintain the head rise at a high level, while the G2 rotor suffers from rather early head rise reduction as shown in figure 5.

Conclusion

In the present paper, the cavitation performances of the waterjet pump blade profile in high-speed vehicle propulsion are concentrated. Refer to the pump performances under high-speed advance, the blade geometries and associated loading situations were studied to improve the pressure distributions as well as the cavitation performances.

1) With the loading point moving backward, the flow turning in the blade passages as well as the work capacity of the blades are obviously weakened, and the deviation angles should be increased to maintain the hydraulic performances of the rotor.

2) The appropriate combination of the design incidence, camber geometry and loading distribution in spanwise could obtain the optimized rotor cavitation performances while maintaining the work capacity, efficiency and other hydraulic performances.
3) With the blade loading optimization in the design stage, the G3 rotor blade appears with superior cavitation performances compared to the G2 rotor blade. And in the severe cavitation situation, the G3 rotor blade still shows relatively superior ability to maintain the head rise at a high level.

Reference

[1] Chen B Y and Reed A M 1990 A design method and an application for contrarotating propellers, DTIC-90/003, David Taylor Research Centre, Bethesda, U. S. A.
[2] Van Gunsteren L A 1971 Application of momentum theory in counterrotating propeller design, *International Shipbuilding Progress*, **206(18)**, pp. 359-372.
[3] Caster E B and LaFone T A 1975 A computer program for the preliminary design of contrarotating propellers, No. SPD-596-01, David W. Taylor Naval Ship Research and Development Centre.
[4] Thurston S and Amsler R C 1966 Review of marine propellers and ducted propeller propulsive devices, *Journal of Aircraft*, **3(3)**, pp.255-261.
[5] Wu H, Tan D, Miorini R L and Katz J 2011 Three-dimensional flow structures and associated turbulence in the tip region of a waterjet pump rotor blade, *Experiments in Fluids*, **51(6)**, pp.1721-1737.
[6] Xiao J P and Jin H 2001 Power effect research on torpedo model with counter-rotation pusher propeller, *Experiments and Measurements in Fluid Mechanics*, **15(3)**, pp. 48-53.
[7] Thad J M, Seth D S and Alan J B 2008 Design of the ONR AxWJ-2 axial flow water jet pump, Hydromechanics Department Report, NSWCCD-50-TR-2008/066.
[8] Zangeneh M 1991 A compressible three-dimensional design method for radial and mixed flow turbomachinery blades. *International Journal for Numerical Methods in Fluids*, **13(5)**, pp. 599-624.
[9] Zangeneh M, Goto A and Harada H 1998 On the design criteria for suppression of secondary flows in centrifugal and mixed flow impellers. ASME, *Journal of Turbomachinery*, **120(4)**, pp. 723-735.
[10] Nishiyama T 1998 *Aerofoil Flow Dynamics* [in Japanese]. Nikkan Kogyo Shimbun.
[11] Cao L L, Watanabe S, Momosaki S, Imanishi T and Furukawa A 2013 Low speed design of rear rotor in contra-rotating axial flow pump. *International Journal of Fluid Machinery and Systems*, **6(2)**, pp. 105-112.
[12] Nishiyama T 1998 *Aerofoil Flow Dynamics* [in Japanese]. Nikkan Kogyo Shimbun.